



Modeling the longitudinal profiles of streamwise velocity in an open channel with a model patch of vegetation

Chunhao Yan¹ · Yuqi Shan^{1,2} · Wei Sun¹ · Chao Liu¹ · Xingnian Liu¹

Received: 13 October 2019 / Accepted: 19 May 2020 / Published online: 2 June 2020
© Springer Nature B.V. 2020

Abstract

This paper proposes a model for predicting the longitudinal profiles of streamwise velocities in an open channel with a model patch of vegetation. The governing equation was derived from the momentum equation and flow continuity equation. The model can estimate the longitudinal profiles of velocities both inside and outside a vegetation patch. Laboratory experiments indicate that the longitudinal profiles of velocities inside a patch and in the adjacent bare channel have the same adjustment distance in the longitudinal direction, but the profiles have different trends because the vegetation drag drives the flow from the patch to the adjacent bare channel. The model considers different dimensionless parameters in two flow adjustment regions upstream of and inside the patch. Sixteen sets of experimental data from different sources are used to verify the model. The model is capable of modeling the longitudinal profiles of velocities inside and outside patches of cylinders or cylinder-like plants. Compared to a previous model, the current model improves the modeling accuracy of longitudinal profiles of velocities.

Keywords Vegetation patch · Analytical model · Partially vegetated channel

1 Introduction

In natural rivers and wetlands, aquatic vegetation often grows in the form of patches with a finite length and width and the size of patches is generally on an order of meters [2, 6, 42–45]. Specifically, the width and length of a patch often ranges between 0.3 and 6 m [8, 22, 37], while the size of a patch is considerably smaller than the size of a natural river, thus forming a partially vegetated channel [50]. Vegetation patches play an important role in trapping sediment and altering the local flow fields in a river system. The interactions among flow, sediment and bed morphology produce different feedbacks inside a vegetation patch and the bare channel (e.g., [8, 37, 41]). Inside a patch, fine

✉ Chao Liu
liuchaoscu@vip.qq.com

¹ State Key Laboratory of Hydraulics and Mountain River Engineering, Sichuan University, Chengdu 610065, China

² Institute for Disaster Management and Reconstruction, Sichuan University, Chengdu 610065, China

suspended sediment and organic matter preferentially deposits in the fully developed flow region due to the low velocity and turbulence [25, 32, 47]. The deposited fine sediment promotes the growth of plants, thus leading to an increase in plant density, which further reduces the velocity and turbulence and enhances sediment deposition [11]. Outside a patch, the flow deflection near the upstream edge of a patch leads to increased velocity in the bare channel, which may produce bed erosion along the side edge of a patch [1, 13]. Because local velocity is related to bedforms (erosion versus deposition), it is important to understand the longitudinal evolution of velocity inside and outside vegetation patches, which can help researchers further identify sediment deposition and erosion regions.

Previous studies investigated how velocities inside and outside a patch develop longitudinally based on indoor flume experiments (e.g., [13, 14, 19, 27–30, 35, 36]). Those studies have confirmed that a model patch of cylinders can lead to flow adjustment associated with velocity variations near the leading edge of the patch, and the results are similar to field observations. In this study, the longitudinal developments of streamwise velocities inside and outside an emergent patch are our focus; therefore, the studies regarding velocity development inside and outside of an emergent patch are reviewed (e.g., [33, 36]). As flow approaches an emergent patch, the velocity in the vegetated region starts decreasing at $x = -L_2$ upstream of the leading edge of the patch ($x = 0$ cm) due to the drag resistance of vegetation. The distance (L_2) between $x = -L_2$ and 0 is defined as the upstream flow adjustment distance. Over a range of flow blockage, $C_d ab = 0.21$ to 8 [29, 36], where C_d is the drag coefficient, a ($=nd$ with vegetation density n and stem diameter d) is the frontal area per patch volume, and b is the half patch width. Inside a patch, the velocity near the upstream edge of the patch continues decreasing over the interior flow adjustment distance, L_3 , which is related to two length scales: $(C_d a)^{-1}$, which represents the drag length scale, and half patch width b , which represents the flow blockage. Beyond $x = L_3$, the flow is fully developed and the velocity becomes constant. Rominger and Nepf [36] assumed that the distance L_3 is the maximum of the two length-scale and could be estimated from Eq. (1) over a range of $C_d ab = 0.21$ to 8.

$$L_3 = (5.5 \pm 0.4) \sqrt{\left(\frac{2}{C_d a}\right)^2 + b^2} \quad (1)$$

Some numerical models can simulate flow entering and exiting a model patch (e.g., [16, 18, 34]). Previous analytical models could only predict lateral profiles of velocities in the fully developed flow region inside patches (e.g., [17, 51]) until a recent work by Liu and Shan [29], who proposed an analytical model for predicting the longitudinal profile of velocity inside a patch. Specifically, Liu and Shan [29] proposed a governing equation from the flow continuity equation and the streamwise momentum equation based on two flow adjustment distances (L_2 and L_3). They divided the longitudinal transect at the centerline of an emergent patch into four regions, and in each region, a predictive equation for velocities was given. However, Liu and Shan [29] assumed that only one dimensionless parameter occurred over two distances near the upstream edge of a patch, which may produce errors. Given this fact, this study considers two different dimensionless parameters in analytical solutions in the upstream and interior flow adjustment regions (L_2 and L_3 , see Sect. 3), which is expected to improve the accuracy of modeling velocities in the vegetated region. In addition, this study employed the flow continuity equation to model the longitudinal profile of velocity in the bare channel adjacent to the patch.

This paper has eight sections. The flume experiment is introduced in Sect. 2. The experimental results and the region division method based on the length scales of flow adjustments upstream of and inside a patch are presented in Sect. 3. The theory of the proposed model is then presented in Sect. 4. Section 5 summarizes the published data for model validation. The modeling results and discussion are presented in Sects. 6 and 7, respectively. Finally, a summary of this study is given in Sect. 8.

2 Experimental methods

Experiments were conducted in a 23-m-long, 2-m-wide and 0.5-m-high straight rectangular channel. The test section was 15-m-long, and the channel bed was horizontal. Across all cases, the flow depth was $H=18$ cm and the mean channel velocity was $U_0=18$ cm/s. Flow depths were monitored by water level gauges along the center of the flume and patch. Though flow depths within patches might change locally, the slope of the water surface over the entire test section was approximately constant (i.e., $S=0.0001$) because the patch occupied less than 15% of the channel bed area ($15\text{ m}\times 2\text{ m}$) (patch size shown in Table 1). The difference between the flow depths at the upstream and downstream edges of the 15-m-long test section was approximately 0.2 cm, producing a negligible variation ($\approx 1\%$) in streamwise velocities. The flow was subcritical at $Fr (= \frac{U_0}{\sqrt{gH}}) \approx 0.14$ and turbulent at $Re (= \frac{U_0 R}{\nu}) \approx 27,500$, in which g is the gravitational acceleration, R is the hydraulic radius and $\nu (=0.01\text{ cm}^2/\text{s})$ is the kinematic viscosity. In this study, we consider only one mean channel velocity U_0 because U_0 does not impact the longitudinal profiles of the streamwise velocity inside and outside an emergent model patch under turbulent flows, i.e., $Re > 2,000$ [52]. A specific material corresponding to Manning's parameter $n_c (=0.013)$ has been reported for PVC baseboard [48]. The Darcy-Weisbach friction factor was estimated based on $f=8gn_c^2/R^{1/3}$ [15, 20].

Model patches of vegetation were constructed using rigid cylinders and placed at the center of the channel. The cylinders do not represent a specific macrophyte but are similar in morphology to a reed, the base of a tree, or a mangrove root (e.g., [23, 40, 49]). Two cylinder diameters ($d=0.4$ and 0.8 cm) were chosen from the range of stem diameters of young plants on floodplains of natural rivers and wetlands, $d=0.1$ to 1 cm, [21, 23, 24, 49]. Specifically, $d=0.4$ was used in cases A1 to A3 while $d=0.8$ was used in cases B1 to B3 (Table 1). The length of the cylinder (30 cm) was greater than the flow depth ($H=18$ cm); thus, in this study, all model patches were emergent. The solid volume fraction, φ , was the same in the two series of cases at $\varphi (= \frac{\pi}{4}nd^2)=0.015$ to 0.045 . This range matches the observed range for cattails in natural rivers and wetlands, where $\varphi=0.001$ to 0.04 [7, 12]. The cylinder density, n , was 0.12 to 0.36 cm^{-2} for cases A1 to A3, producing a frontal area per patch volume of $a (=nd)=0.048$ to 0.144 cm^{-1} . With a larger diameter ($d=0.8$ cm), cases B1 to B3 had smaller $n (=0.03$ to $0.09\text{ cm}^{-2})$ and $a (=0.024$ to $0.072\text{ cm}^{-1})$ values compared to those in cases A1 to A3. Each model patch was designed to be sufficiently long to create a fully developed flow region inside the patch. That is, the length of the model patch, L , was greater than the interior adjustment length, L_3 , (i.e., $L > L_3$). The half patch width, b , ranged between 30 and 40 cm. The experimental parameters are summarized in Table 1.

The longitudinal, lateral and vertical directions are denoted as x , y and z , respectively. $x=0$ cm indicates the upstream edge of the patch; $y=0$ cm indicates the centerline of the flume and model patch, and $z=0$ cm indicates the surface of the channel bed. Velocities

Table 1 Summary of the experimental parameters in six cases

Case	d (cm)	f	n	n (cm^{-2})	a (cm^{-1})	$C_d ab$	φ	dx (cm)	dy (cm)	L (cm)	b (cm)	L_2 (cm)	L_3 (cm)	K_2	K_3	$RMSE$ (cm/s)	$RMSE/U_0$ (%)
A1	0.4	0.025	0.12	0.048	1.92	0.015	4.6	3.6	500	40	60 ± 10	350 ± 10	2	4	0.9	5.2	
A2	0.4	0.025	0.18	0.072	2.16	0.023	3.8	3	400	30	50 ± 10	300 ± 20	2	2	1.0	5.4	
A3	0.4	0.025	0.36	0.144	4.32	0.045	2.6	2.2	300	30	30 ± 10	210 ± 15	1.5	2	1.0	5.5	
B1	0.8	0.025	0.03	0.024	0.96	0.015	9.2	7.2	450	40	50 ± 10	390 ± 20	2	2	0.8	4.2	
B2	0.8	0.025	0.045	0.036	1.08	0.023	7.4	6	400	30	30 ± 10	330 ± 20	3	1	0.8	4.2	
B3	0.8	0.025	0.09	0.072	2.16	0.045	5.2	4.4	300	30	50 ± 10	230 ± 20	2	4	0.6	3.2	

Where d is the cylinder diameter; f ($= 8gn_c^2/R^{1/3}$) is the Darcy-Weisbach friction factor, in which n_c and R are the Manning's parameter and channel hydraulic radius, respectively; n is the cylinder density; a ($= nab$) is the frontal area per patch volume; C_d (≈ 1) is the drag coefficient; $C_d ab$ is the flow blockage; φ is the solid volume fraction; dx and dy are the longitudinal and lateral distances between the in-row and in-line neighboring cylinders, respectively; L and b are the length and half width of a vegetation patch, respectively; L_2 is the distance between the position at which the velocity is 95% of the mean channel velocity, U_{95} , and the upstream edge of the patch ($x=0$ cm); and L_3 is the distance between the upstream edge of the patch ($x=0$ cm) and the position at which the velocity is constant inside the patch. K_2 and K_3 are dimensionless parameters. $RMSE$ is the root mean square error, which is estimated from Eq. (2)

were recorded using a Sontek ADV equipped with a downward-looking probe. When the vertical profiles of the velocities were measured, the velocities in the 5 cm blind space near the water surface were measured by the ADV equipped with an upward-looking probe. At each point, the measurement time and frequency were set as 150 s and 50 Hz, respectively. The raw data were de-spiked using the method of Gorning and Nikora (2002), and raw data with correlations less than 70% and a signal to noise ratio smaller than 15 db were removed. The remaining instantaneous velocities were decomposed into time-averaged velocities (U , V and W) using a MATLAB code. Inside the patch and the bare channel, the difference between the depth-averaged velocity, U_d , and the mid-depth velocity, U , at mid-depth ($z=H/2$) was 3% on average. To facilitate a large number of individual velocity measurements per trial, it is reasonable to use the mid-depth velocity, U , as the depth-averaged velocity, U_d . Inside a model patch, velocities were measured at the middle depth ($z=H/2$) along the centerline of the flume and model patch ($y=0$ cm). The longitudinal interval of two x -positions was 10 to 15 cm depending on the stem density and patch length. The interval is comparable or a few times greater than the longitudinal distance between in-row neighboring cylinders, dx . At each x -position, a characteristic region was considered (the dashed line box in Fig. 1a), in which two velocities were measured at $y=0$ cm and $dy/4$, with the lateral spacing between two neighboring cylinders, dy . In each characteristic region, the mean of two velocities differed from the spatial mean of the velocities by less than 12%, therefore, it was reasonable to use the mean of two velocities as the local spatial mean velocity, which includes the influence of spatial flow heterogeneity. We measured two velocities at $y=0$ cm and $dy/4$ in a characteristic region at each x -position. In addition, lateral profiles of velocities were measured at selected positions in which the lateral interval between two neighboring positions was 10 cm. Specifically, the lateral profiles of velocities were measured at $x=180$ and 420 cm for case A1 and at $x=180$ and 300 cm for cases A2 and A3, while they were measured at $x=100, 150, 200, 250, 300, 400$ and 420 cm for case B1 and at $x=0, 50, 100, 150, 200,$ and 300 for cases B2 and B3. In the bare channel, longitudinal profiles of velocities were measured at $y/b=1.5$ ($b=40$ cm) for case A1 and B1 but at $y/b=2.2$ ($b=30$ cm) for cases A2 and A3 because the lateral profiles of velocities in the bare channel depend on the width of the bare channel and the shear layer. For cases B2 and B3, the mean velocity of the bare channel, U_{bare} , was calculated from the detailed velocity measurements.

To compare the difference between the modeled and measured velocities, the root mean square error, $RMSE$, was defined as follows:

$$RMSE = \sqrt{\frac{1}{N} \sum_{i=1}^N (U_{d(m)} - U_{d(p)})^2} \quad (2)$$

where N is the number of measurements and modeled values in each case, $U_{d(m)}$ is the measured streamwise velocity, and $U_{d(p)}$ is the predicted streamwise velocity.

3 Experimental results

3.1 Longitudinal velocity profiles

The longitudinal profiles of the depth-averaged streamwise velocity, U_d , at the centerline of the patch ($y/b=0$) and near the centerline of the bare channel ($y/b=1.5$) for case B1

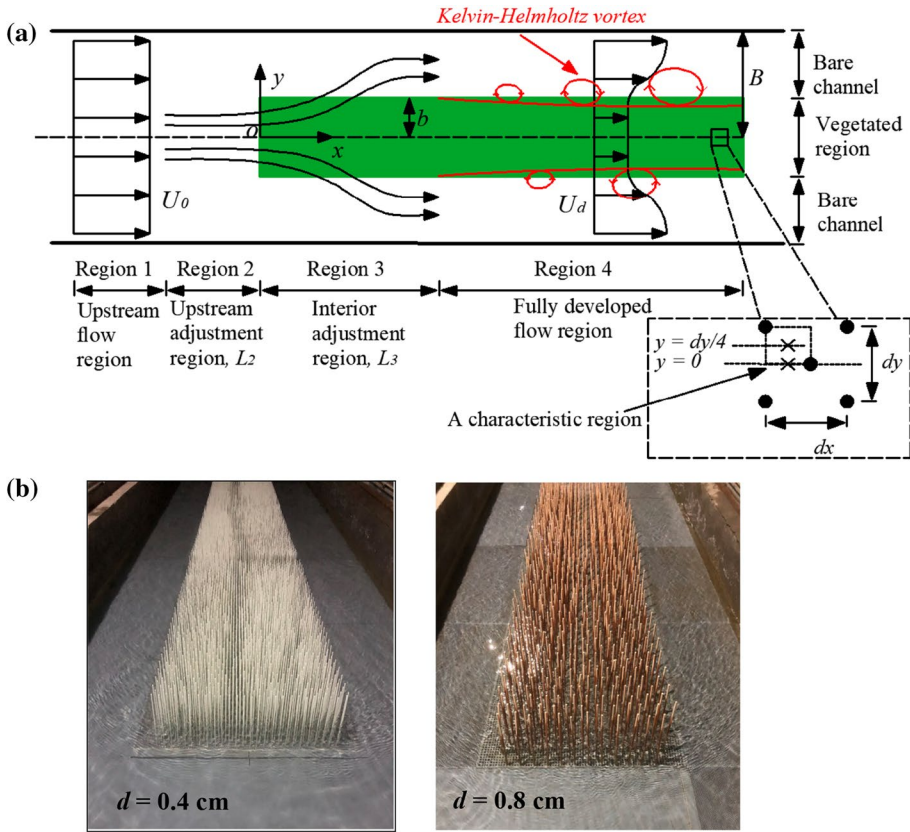


Fig. 1 **a** Sketch of flow development within and around an emergent patch of model vegetation. The green rectangle indicates a cylinder array. The vegetated region and bare channel are divided at the lateral transect. Four regions are divided at the longitudinal transect based on two flow adjustment distances (L_2 and L_3). At each x position, velocities were measured at $y=0$ cm and $dy/4$ in a characteristic region. dx and dy are the intervals between the in-row and in-line neighboring cylinders, respectively. **b** Images of model patches with cylinder diameters of $d=0.4$ cm and $d=0.8$ cm, which correspond to cases A1 and B1, respectively. The flow direction is from bottom to top

(black and red squares, respectively) are plotted in Fig. 2. The profiles of the velocities in the vegetated region and bare channel share the same flow adjustment distances (L_2 and L_3) but have different tendencies. We take the profile in the vegetated region (black squares in Fig. 2) as an example to discuss the flow adjustment distances and velocity trends.

U_d far from the upstream edge of the model patch ($x < -L_2$, Region 1) was not disturbed by the patch and was the same as the mean channel velocity, U_0 . As the flow approached the patch ($0 > x > -L_2$, Region 2), the velocity upstream of the patch started decreasing because the flow was deflected laterally to the bare channel due to the patch blockage, resulting in increasing velocity in the bare channel. There is a length scale for velocity decay upstream of the patch, L_2 , which is defined as the distance between the position at which U_d is 95% of U_0 and the upstream edge of the patch ($x/b=0$). This length scale, L_2 , is the same under increasing velocity in the bare channel because the velocity at any transect along the channel obeys the continuity equation at $-L_2 \leq x \leq 0$ cm (Region 2), resulting in

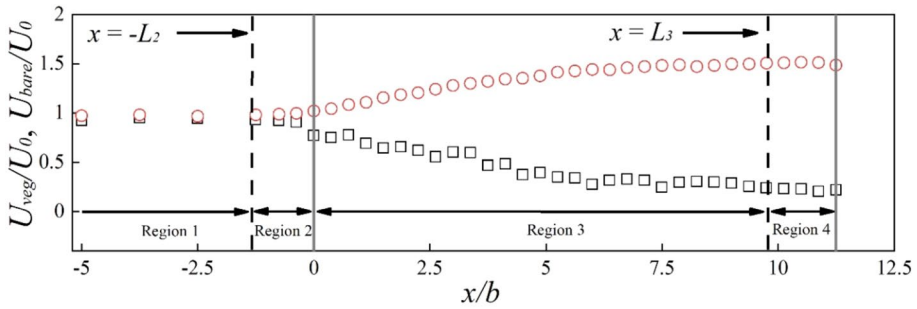


Fig. 2 Depth-averaged streamwise velocities, U_d , normalized by the mean channel velocity U_0 ($= 18$ cm/s), versus the longitudinal position, x , normalized by the half patch width, b , at the centerlines of the vegetated region (black squares) and bare channel (red circles) based on the data from case B1 ($d=0.8$ cm and $\varphi=0.015$). Two length scales (L_2 and L_3) are defined based on the longitudinal profiles of velocities. L_2 is the distance between the position at which U_d is 95% of U_0 and the upstream edge of the patch ($x/b=0$). L_3 is the distance between the upstream edge of the patch ($x/b=0$) and the position at which U_0 becomes constant inside the patch. Over L_2 and L_3 , velocities decrease in the vegetated region but increase in the bare channel because the flow is deflected from the vegetated region to the bare channel. Four regions (Regions 1 to 4) are divided based on two length scales

increasing velocity over L_2 (Fig. 2). Similarly, when the flow enters a model patch, U_d continues decreasing until the pressure gradient balances the drag of vegetation. The flow that is deflected laterally from the vegetated region to the bare channel flow results in increased velocity in the bare channel (Region 3). The length scale for velocity development in the vegetated region and the bare channel is the same and is defined as L_3 , which is the distance between the upstream edge of the patch ($x/b=0$) and the position at which the velocity is constant. For case B1, $L_2=50 \pm 10$ cm ($L_2/b=1.3$ with $b=40$ cm) and $L_3=390 \pm 20$ cm ($L_3/b=9.8$), as noted in Fig. 2. Additionally, across six cases, although the cylinder diameters in series A ($d=0.4$ cm) and series B ($d=0.8$ cm) are different, L_2 and L_3 values are approximately equal within a given uncertainty range in cases with the same solid volume fraction φ (see Table 1). For example, for case A2 ($\varphi = 0.023$), $L_2=50 \pm 10$ cm and $L_3=300 \pm 20$ cm, which are the same as those ($L_2=30 \pm 10$ cm and $L_3=330 \pm 20$ cm) for case B2 ($\varphi = 0.023$). This finding indicates that compared to d , φ is a more important factor for determining the flow adjustment length scales (L_2 and L_3).

3.2 Lateral velocity profiles

The lateral profile of the depth-averaged streamwise velocity, U_d , in the fully developed flow region inside the patch ($x=420$ cm) is taken as an example and is plotted in Fig. 3 based on the data from case B1. First, the measurements confirm that velocities are symmetric across the centerline of the flume and patch ($y/b=0$); thus, it is reasonable to measure velocity profiles over a half flume. Second, for a half flume ($2.5 \geq y/b \geq 0$, the right side in Fig. 3), two regions can be established, denoted as Region A (the vegetated region, $1 \geq y/b \geq 0$, with the half patch width $b=40$ cm) and Region B (the bare channel, $2.5 \geq y/b \geq 1$, with the half channel width $B=100$ cm). The mean velocities in Region A and Region B are defined as U_{veg} ($= \frac{1}{b} \int_0^b U_d dy$) and U_{bare} ($= \frac{1}{B-b} \int_b^B U_d dy$), respectively, which are denoted the black and red dashed arrow lines, respectively. U_{veg} is approximately the same as U_d at the centerline of the vegetated region ($y/b=0$). Taking case B1 as an

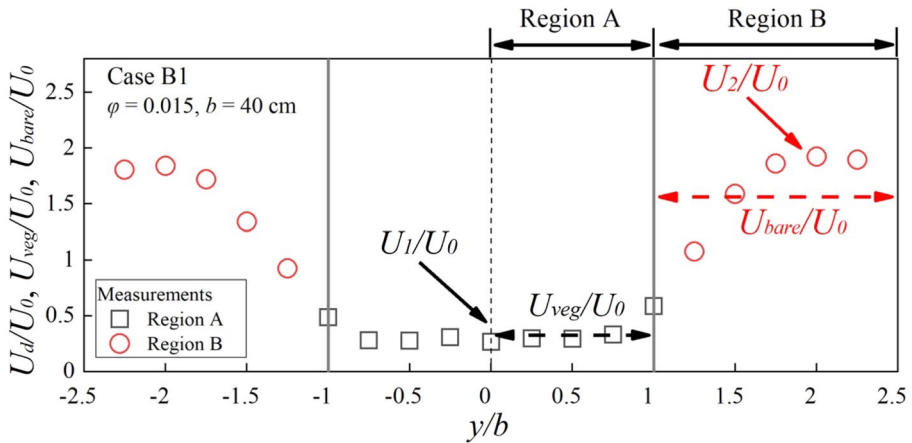


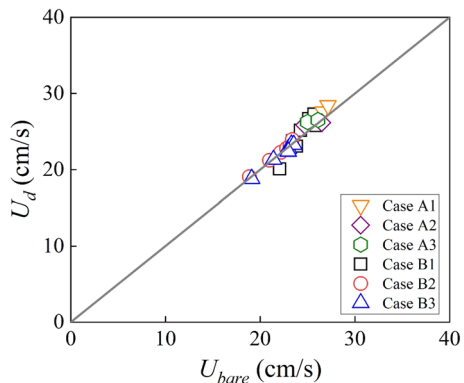
Fig. 3 Depth-averaged streamwise velocities, U_d , normalized by the mean channel velocity U_0 ($= 18$ cm/s) plotted versus the lateral position, y , normalized by the half patch width, b , based on the data at $x=420$ cm in case B1. U_d/U_0 in Region A (the vegetated region, $1 \geq y/b \geq 0$) and Region B (the bare channel, $2.5 \geq y/b \geq 1$) is denoted black squares and red circles, respectively. U_{veg} and U_{bare} are the mean velocities in Region A (the black dashed array line) and that in Region B (the red dashed array line), respectively. U_1 and U_2 are steady velocities in the vegetated region and bare channel, respectively. b ($= 40$ cm) is the half patch width, and B ($= 100$ cm) is the half channel width

example (Fig. 3), U_{veg} (the black dashed arrow line) is 4% greater than U_d at $y=0$ cm, thus, it is reasonable to assume that U_{veg} is the same as U_d at the centerline of Region A.

In Region B (the bare channel), the velocity was measured at $y/b=1.5$. The difference between the measured U_{bare} (calculated from $\frac{1}{B-b} \int_b^B U_d dy$) and the velocity at $y/b=1.5$ is 4%; therefore, it is reasonable to assume that U_{bare} is the same as U_d at $y/b=1.5$ for case B1. Similarly, velocity was measured at $y/b=1.5$ for case A1 while at $y/b=2.2$ for cases A2 and A3. The measurement position was different because the lateral profile of velocities depends on the width of the bare channel and of the shear layer. For all six cases, at different x positions, the difference between U_{bare} and U_d at $y/b=1.5$ to 2.2 in the bare channel is less than 9% (Fig. 4), indicating that the difference is negligible.

In addition, the steady velocity in the vegetated region and bare channel is defined as U_1 and U_2 , respectively (Fig. 3), and the velocity difference, λ ($= \frac{U_2 - U_1}{U_2 + U_1}$), is used to evaluate the

Fig. 4 Comparison between the mean velocity in the bare channel, U_{bare} , and the local depth-averaged velocity, U_d , at $y/b=1.5$ or 2.2 . In the bare channel, the local velocity, U_d , was measured at $y/b=1.5$ for cases A1 and B1 and at $y/b=2.2$ for cases A2, A3, B2 and B3. Each symbol indicates a velocity measurement at a transect. The x position of each transect is introduced in Sect. 2. Across the six cases, the difference between U_{bare} and U_d is less than 9%



formation of the Kelvin–Helmholtz vortices along the side edge of an emergent model patch. Caroppi et al. [3] reported that in the fully developed flow region ($x > L_3$), the Kelvin–Helmholtz vortices occurred at $\lambda \geq 0.4$. In this study, U_1 and U_2 were extracted from the transects in the fully developed flow region ($x > L_3$). For example, for case B1 (Fig. 3), $U_1 = 4.8$ cm/s and $U_2 = 33.1$ cm/s, resulting in $\lambda = 0.7$. For the other five cases (A1, A2, A3, B2 and B3), $\lambda = 0.8$ to 0.9 . The λ ($= 0.7$ to 0.9) values are greater than the observed threshold ($= 0.4$), suggesting the Kelvin–Helmholtz vortices occurred in the six cases.

4 Theory

4.1 Analytical solution in the vegetated region

For an incompressible fluid, the force acting on a unit volume of water body (left-side of Eq. (3)) balances the inertial force (right-side of Eq. (3)) in the streamwise direction, thus, the momentum equation in an open channel with vegetation can be expressed as follows:

$$\rho f_x + \frac{\partial \tau_{xx}}{\partial x} + \frac{\partial \tau_{yx}}{\partial y} + \frac{\partial \tau_{zx}}{\partial z} = \rho \left(\frac{\partial U}{\partial t} + \frac{\partial U}{\partial x} U + \frac{\partial U}{\partial y} V + \frac{\partial U}{\partial z} W \right) \tag{3}$$

where x , y and z are the streamwise, lateral and vertical directions, respectively; U , V and W are the time-averaged velocity components corresponding to the x , y and z directions, respectively; ρ is the flow density; and τ is the Reynolds shear stress. For steady flow, $\frac{\partial U}{\partial t} = 0$. Inside the model patch, the lateral gradient of velocity (shear stress) is negligible; therefore, $\frac{\partial U}{\partial y} = 0$ and $\frac{\partial \tau_{yx}}{\partial y} = 0$ [29].

The shear stress, τ_{xx} , is defined as follows:

$$\tau_{xx} = -p + 2\rho\varepsilon \frac{\partial U}{\partial x} \tag{4}$$

where p ($= -\rho gh$) is the fluid pressure and ε is the eddy viscosity. f_x is the drag force due to vegetation in the streamwise direction and is defined as follows:

$$f_x = \frac{1}{2} C_d a U^2 \tag{5}$$

The flow continuity equation is shown as follows:

$$\frac{\partial U}{\partial x} + \frac{\partial V}{\partial y} + \frac{\partial W}{\partial z} = 0 \tag{6}$$

Combining Eqs. (3), (4), (5) and (6), one can obtain the following governing equation:

$$-\frac{1}{2} \rho C_d a U^2 + 2\rho\varepsilon \frac{\partial U}{\partial x^2} + \rho g S + \frac{\partial \tau_{zx}}{\partial z} = \rho \frac{\partial U^2}{\partial x} + \rho \frac{\partial U W}{\partial z} \tag{7}$$

In Eq. (7), ε has a magnitude of cm^2/s and varies depending on the flow conditions. It is reasonable to assume that $\varepsilon = KUH$, where K is a dimensionless parameter (e.g., Liu and Shan [29]). The Reynolds shear stress, τ_{zx} , acting on the x - z panel is ≈ 0 N/cm^2 at the water surface, and $z = H$ and is equal to the bed shear stress, τ_b , at the channel bed ($z = 0$ cm). The bed shear can be calculated from $\tau_b = \rho U_*^2$, with the bed shear velocity,

$U_* \left(= \sqrt{\frac{f}{8}} U_d \right)$, in which f is the Darcy-Weisbach friction factor. At the water surface, $z=H$, and the channel bed, $z=0$ cm, the time-averaged velocity in the vertical direction is $W \approx 0$ cm/s.

The depth-averaged governing equation Eq. (8) in an open channel with a model vegetation patch can be obtained by integrating Eq. (7) over the water depth, H .

$$-\frac{1}{2} \rho H C_d a U_d^2 + \rho K H^2 \frac{\partial U_d^2}{\partial x^2} + \rho g S H - \rho \frac{f}{8} U_d^2 = \rho H \frac{\partial U_d^2}{\partial x} \tag{8}$$

For the bare channel without vegetation, $a=0$ cm⁻¹ in Eq. (8).

The longitudinal transect upstream of and within a model patch is divided into four regions (see Sect. 3.1 and Fig. 2 for details). Liu and Shan [29] reported that in two adjustment regions (Regions 2 and 3), the dimensionless parameter is assumed to be the same in the two regions. However, the dimensionless parameter K should be different in Regions 2 and 3 because ϵ and H are the same in a specific case but U is different in Regions 2 and 3, resulting in two different K parameters (K_2 and K_3) based on $\epsilon = KUH$. For simplicity, the two parameters (K_2 and K_3) are considered constant in each region and are modified as calibration parameters until the best results are obtained. One goal of this study is to examine whether the modeling of the longitudinal velocity profiles inside patches can be improved by using two different parameters in Regions 2 and 3. The analytical solutions for Eq. (8) in Regions 1 to 4 are introduced below.

In Region 1 ($x \leq -L_2$, Fig. 2), $U_{d(1)}$ is equal to the mean channel velocity, U_0 , thus, Eq. (8) can be simplified as $\rho g S H - \rho \frac{f}{8} U_{d(1)}^2 = 0$. The subscript of $U_{d(i)}$ indicates the number of the region ($i=1-4$). The analytical solution for Region 1 is as follows:

$$U_{d(1)} = \sqrt{\frac{8gSH}{f}} \tag{9}$$

In Region 2 ($-L_2 \leq x \leq 0$), the analytical solution of $U_{d(2)}$ is

$$U_{d(2)} = \sqrt{A_1 e^{r_1 x} + A_2 e^{r_2 x} + \frac{8gSH}{f}} \tag{10}$$

where $r_{1,2} = \frac{1}{2K_2 H} \pm \frac{1}{2K_2 H} \sqrt{1 + \frac{1}{2} K_2 f}$ and A_1 and A_2 are unknown constants.

In Region 3 ($0 \leq x \leq L_3$), the analytical solution of $U_{d(3)}$ is obtained as follows:

$$U_{d(3)} = \sqrt{A_3 e^{r_3 x} + A_4 e^{r_4 x} + \frac{8gSH}{4C_d a H + f}} \tag{11}$$

where $r_{3,4} = \frac{1}{2K_3 H} \pm \frac{1}{2K_3 H} \sqrt{1 + \frac{1}{2} K_3 (4C_d a H + f)}$ and A_3 and A_4 are unknown constants.

In Region 4 ($x \geq L_3$), $U_{d(4)}$ becomes constant; therefore, Eq. (8) is simplified as $-\frac{1}{2} \rho H C_d a U_{d(4)}^2 + \rho g S H - \rho \frac{f}{8} U_{d(4)}^2 = 0$. Moreover, $U_{d(4)}$ can be obtained with the following formula:

$$U_{d(4)} = \sqrt{\frac{8gSH}{4C_d a H + f}} \tag{12}$$

To obtain the four unknown constants (A_1, A_2, A_3 and A_4) in Eqs. (10) and (11), four boundary conditions are needed. First, velocity continuity and velocity gradient continuity conditions must be met at the interface of Regions 2 and 3, corresponding to $U_{d(2)} = U_{d(3)}$ and $\frac{\partial U_{d(2)}}{\partial x} = \frac{\partial U_{d(3)}}{\partial x}$, respectively. Additionally, due to the flow continuity, $U_{d(1)} = U_{d(2)}$ at the interface of Region 1 and 2 for $x = -L_2$ and $U_{d(3)} = U_{d(4)}$ at the interface of Region 3 and 4 for $x = L_3$.

In Region A (the vegetated region), the velocities modeled by Eqs. (9)–(12) at the centerline are equivalent to or slightly smaller than the spatial mean velocity of the vegetated region, U_{veg} (see Sect. 3), due to lateral momentum exchange near the interface of the patch and bare channel, which results in enhanced local velocities, thus, it is reasonable to assume that the modeling velocities of Eqs. (9)–(12) represent the mean velocity of the vegetated region, U_{veg} .

4.2 Analytical solution in the bare channel

In the following text, we only consider U_{veg} in Region A (the vegetated region) and U_{bare} in Region B (the bare channel). The mean velocities (U_{veg} and U_{bare}) in Regions A and B over half a channel must satisfy the flow continuity equation.

$$BU_0 = bU_{veg} + (B - b)U_{bare} \quad (13)$$

Because the longitudinal profile of U_{veg} ($= U_d$) in the vegetated region can be modeled using Eqs. (9) – (12), based on Eq. (13), the longitudinal velocity profiles in the bare channel U_{bare} can be modeled using Eq. (14).

$$U_{bare} = (BU_0 - bU_{veg})/(B - b) \quad (14)$$

In this study, the shear between the vegetated region and the bare channel is ignored. When the width of the bare channel is comparable or smaller than the width of the shear layer, the consistency between the modeling and measured velocities in the bare channel depends on the width of the channel.

5 Published experimental data for model validation

The experimental data from our study and published studies (i.e., [10, 31, 33, 46, 52]) are used to verify the proposed model over a wide range of φ ($=0.003$ to 0.1), b/B ($=27$ to 75%) and U_0 ($=5$ to 29 cm/s) values. The details of those studies were reported in the respective papers. For convenience, brief descriptions of those studies are given as follows.

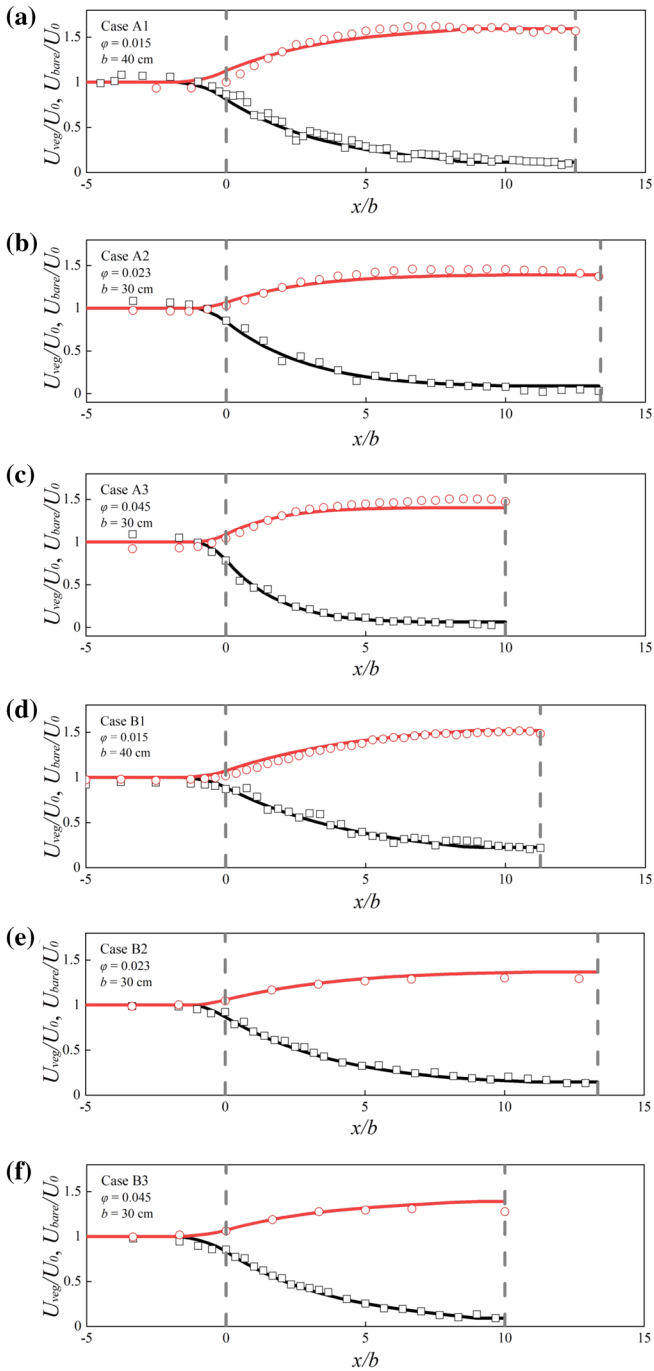
- (1) White and Nepf [46] and Zong and Nepf [52] performed experiments in the same flume, which was 16 m long and 1.2 m wide. In two studies, 40-cm-wide patches were constructed using rigid cylinders with a diameter of $d=0.6$ cm, and patches were sufficiently long to create a fully developed flow region inside the patches. In the case of White and Nepf [46], the flow depth was $H=6.6$ cm, and the mean channel velocity was $U_0=7.8$ cm/s. The frontal area per canopy volume was $a=0.088$ cm⁻¹, yielding a solid volume fraction of $\varphi=0.045$. Velocities were measured along transects at $x=33, 99, 195, 386, 513,$ and 577 cm (see Fig. 3 in White and Nepf [46]). Based on those velocities, U_{veg} and U_{bare} were calculated. In the case of Zong and Nepf [52], $H=12$

Fig. 5 Comparison between the modeled and measured longitudinal profiles of U_{veg} and U_{bare} normalized by the mean channel velocity, U_0 , in the vegetated region (Region A, black line and points) and in the bare channel (Region B, red line and points) based on the data from our study. Cases A1 to A3 had a cylinder diameter of $d=0.4$ cm (see subplots a–c). Cases B1 to B3 had $d=0.8$ cm (see subplots d–f). The lines and points are the modeling results and velocity measurements, respectively. b is the half patch width. φ is the solid volume fraction. The region between the two gray dashed lines indicates a model patch. The parameters are summarized in Table 1

- and 14 cm, which correspond to $U_0=5.0$ and 11.6 cm/s, respectively. The authors constructed two patches with $a=0.04$ and 0.21 cm^{-1} , corresponding to $\varphi=0.02$ and 0.1, respectively. Velocities were measured along a longitudinal transect at the centerlines of the model patches ($y=20$ cm) and along different selected lateral transects ($x=675$ to 800 cm) (see Fig. 7 in Zong and Nepf [52]).
- (2) Maji et al. [31] performed experiments in a 12-m-long, 0.9-m-wide and 0.6-m-deep rectangular channel with a bed slope of $S=0.002$. For this channel, $H=15$ cm and $U_0=29$ cm/s. A 0.8-m-long and 0.12-m-wide emergent patch was constructed with cylinders of $d=0.64$ cm. For the patch, $a=0.022$ cm^{-1} and $\varphi=0.01$. The test section of the flow was 3 m long, and vertical profiles of the streamwise velocities were measured at six transects between $x/b=0$ and 7.5 (see Fig. 2 in their paper).
 - (3) Ben Meftah and Mossa [33] performed velocity measurements in a 15-m-long, 4-m-wide and 0.4-m-deep flume with a horizontal bed. In the case $H=18$ cm and $U_0=13.9$ cm/s, an emergent model patch that was 3-m-long and 3-m-wide was constructed using steel cylinders with $d=0.3$ m. For the patch, $a=0.012$ cm^{-1} and $\varphi=0.003$. The vertical profiles of streamwise velocities were measured at thirteen lateral transects between $x/b=0$ and 1.2 (see Figs. 2 and 4 in their paper, from which the velocity data were extracted).
 - (4) Devi et al. [10] performed experiments in a 20-m-long, 1-m-wide and 0.72-m-deep flume with $S=0.0015$. Additionally, $H=12$ cm, and $U_0=27$ cm/s. The no seepage case was considered. A 5-m-long and 0.5-m-wide emergent vegetation patch was constructed from natural rice stems (*O. sativa*) with $d=0.1$ to 0.3 cm. For the patch, $a=0.06 \pm 0.03$ cm^{-1} and $\varphi=0.010 \pm 0.006$. The vertical profiles of streamwise velocities measured at the centerlines of patches ($y/b=0.5$) and adjacent to the bare channel ($y=75$ cm, $y/b=0.75$) were extracted to verify the proposed model (data from Fig. 3 in Devi et al. [10]).

6 Modeling results

First, velocity measurements from this study were used to verify the model. In Fig. 5, the modeled longitudinal profiles of U_{veg} and U_{bare} , normalized by U_0 , were compared to the measured velocities (cases A1 to A3 and B1 to B3) in the vegetated region (black lines and points) and in the bare channel (red lines and points). In the $d=0.4$ cm cases (A1 to A3) and $d=0.8$ cm cases (B1 to B3), the modeled longitudinal profiles of the streamwise velocities (lines in Fig. 5) agree well with the measured velocities (points in Fig. 5) in both the vegetated region and the bare channel. Furthermore, the proposed model is compared to a previous model [29] based on the data from case A1 (Fig. 6). Inside the patch, the results of the current model are closer to the velocity measurements because two different parameters are used in the two flow adjustment regions. The mean velocities of the bare



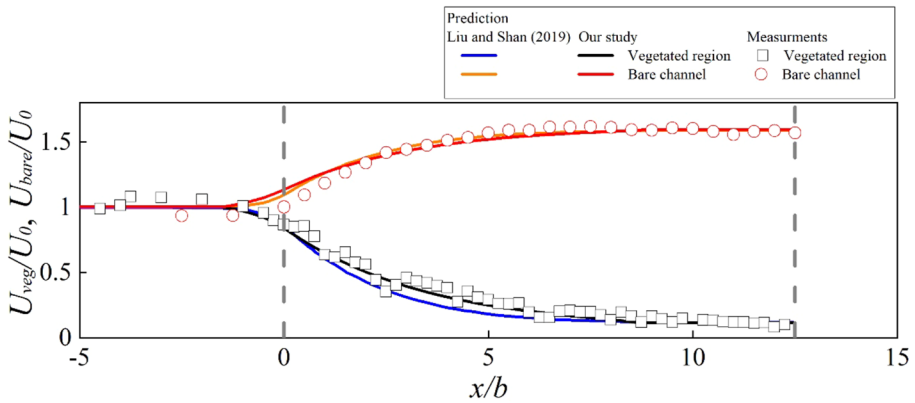


Fig. 6 Modeling the longitudinal profiles of U_{veg} normalized by the mean channel velocity, U_0 , versus the measurements in the vegetated region based on the data from case A1. Inside the model patch, the modeling results of the proposed model (the black line) are closer to measurements (black squares) than the results of Liu and Shan [29] (the blue line). For both methods, the mean velocities in the bare channel, U_{bare} , were estimated from Eq. (14). The region between the two gray dashed lines indicates the patch. The parameters are summarized in Table 1

channel are modeled using Eq. (14). The current model and the previous model present approximately equivalent velocities.

Second, the data from White and Nepf [46] and Zong and Nepf [52] were used to perform validations. Over a wide range of mean channel velocities ($U_0=5$ to 11 cm/s) and solid volume fractions ($\varphi=0.02$ to 0.1), the proposed model yields longitudinal profiles of U_{veg} and U_{bare} (lines in Fig. 7) that are in good agreement with the measured velocities (points in Fig. 7) in both the vegetated region (squares in Fig. 7) and the bare channel (circles). Additionally, this model used two different dimensionless parameters in Regions 2 and 3, therefore, accurate modeling was obtained, with an average RMSE of 0.5 cm/s for cases A1 to A3 and for the data of Zong and Nepf [[52]]. Liu and Shan [29] performed predictions in the same cases but used only one dimensionless parameter, thus, they had higher RMSEs ($=0.7$ cm/s). The above comparison confirms that the proposed model improves the modeling accuracy of longitudinal velocity profiles compared to the previous model.

Third, the data from Maji et al. [31] and Ben Mefteh and Mossa [33] were used to further verify the model. In the two studies, model patches were not long enough to create a fully developed flow region inside a patch ($L < L_3$), which is different from the situation in our study and those investigated by White and Nepf [46] and Zong and Nepf [52]. Liu and Shan [29] found that the length of an emergent patch does not impact the lateral flow adjustment near the upstream edge of the patch, and consequently, the length of an emergent patch does not influence the longitudinal velocity profile upstream of and inside a patch. Thus, the proposed model can be effectively used to obtain longitudinal velocity profiles, and parts of the profiles should match measurements. Over ranges of $U_0=(14$ to 29 cm/s) and $\varphi=(0.003$ to 0.01), the proposed model yielded longitudinal profiles of U_{veg} and U_{bare} (lines in Fig. 8) that generally match the measured velocities (points in Fig. 8) in the vegetated region and bare channel, with RMSEs = 1.3 to 1.6 cm/s.

Finally, the model was verified using measured velocities inside and outside of a natural patch constructed of natural rice stem [10]. The patch was long enough to achieve a

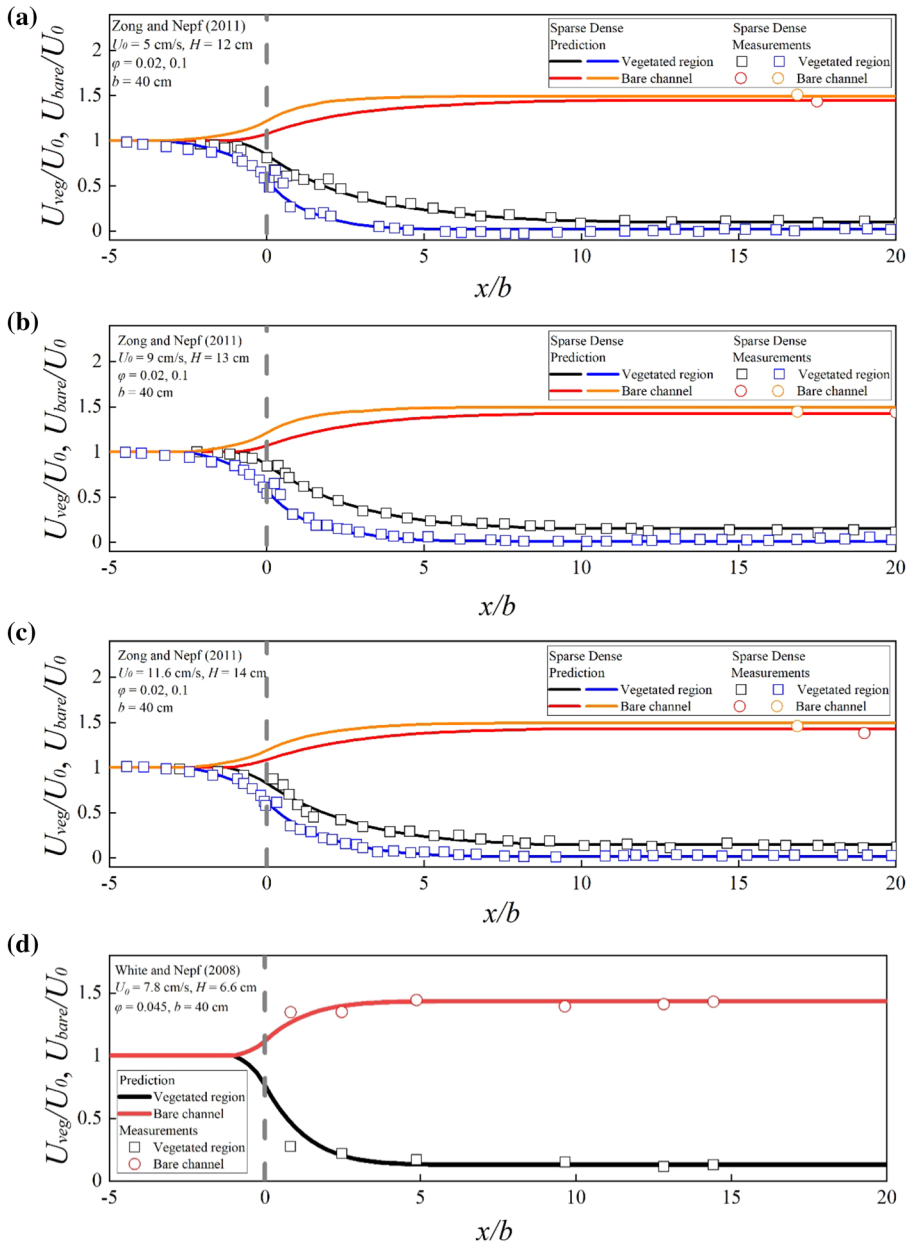


Fig. 7 Modeling the longitudinal profiles of U_{veg} and U_{bare} normalized by the mean channel velocity, U_0 , versus measurements in the vegetated region and bare channel based on the data from Zong and Nepf [52] (subplot a–c) and White and Nepf [46] (subplot d). Each subplot of Zong and Nepf [52] contains sparse ($\varphi=0.02$) and dense patches ($\varphi=0.1$). U_0 is the mean channel velocity; H is the flow depth; b is the half patch width; and φ is the solid volume fraction. The vertical gray dashed line is the upstream edge of the patch. The parameters are summarized in Table 2

Table 2 Summary of the experimental parameters from the published literature

Case	d (cm)	f	H (cm)	U_0 (cm/s)	n (cm ⁻²)	a (cm ⁻¹)	$C_d ab$	ϕ	L (cm)	b (cm)	L_2 (cm)	L_3 (cm)	K_2	K_3	$RMSE$ (cm/s)	$RMSE/U_0$ (%)
Maji et al. [31]	0.64	0.048	15	29	0.035	0.022	0.22	0.01	81.6	12.3	12	500	0.2	7	1.6	5.7
Mehtah and Mossa [33]	0.3	0.073	18	13.9	0.04	0.012	1.8	0.003	300	150	150	1100	0.5	26	1.3	9.7
Devi et al. [10]	0.2	0.05	12	27	0.3	0.06	3	0.01	500	50	50	320	2	25	0.9	3.2
White and Nepf [46]	0.65	0.04	6.6	7.8	0.135	0.088	3.52	0.045	1300	40	40	220	5	2	0.5	7.1
Zong and Nepf [52]	0.6	0.048	12	5	0.067	0.04	1.6	0.02	1000	40	40	350	3	1.8	0.2	4.8
	0.6	0.048	13	9	0.067	0.04	1.6	0.02	1000	40	40	350	3	2	0.2	2.7
	0.6	0.048	14	11.6	0.067	0.04	1.6	0.02	1000	40	40	350	4	2	0.4	3.4
	0.6	0.048	12	5	0.35	0.21	8.4	0.1	1000	40	40	240	6	4	0.2	4.6
	0.6	0.048	13	9	0.35	0.21	8.4	0.1	1000	40	40	240	6	4	0.3	3.9
	0.6	0.048	14	11.6	0.35	0.21	8.4	0.1	1000	40	40	240	6	7	0.3	2.3

H is the flow depth, and U_0 is the mean channel velocity. The other notations have the same definitions as those in Table 1

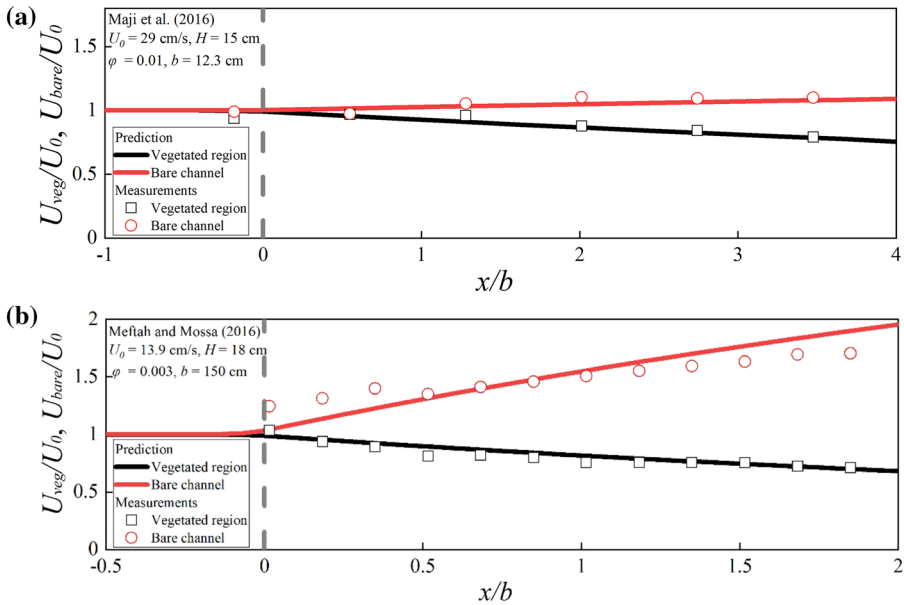


Fig. 8 Modeling the longitudinal profiles of U_{veg} and U_{bare} normalized by the mean channel velocity, U_0 , versus the measurements in the vegetated region (black line and points) and in the bare channel (red line and points) based on the data from Maji et al. [31] and Ben Meftah and Mossa [33] (see Table 2). U_0 is the mean channel velocity, H is the flow depth, b is the half patch width; and φ is the solid volume fraction. The vertical gray dashed line is the upstream edge of the patch

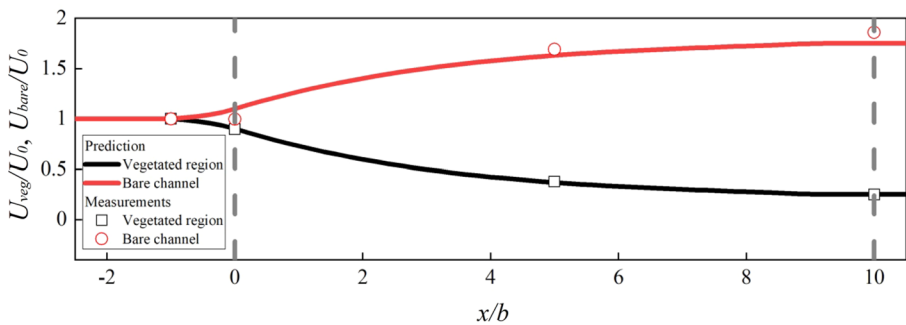


Fig. 9 Modeling the longitudinal profiles of U_{veg} and U_{bare} normalized by the mean channel velocity, U_0 , versus measurements in the vegetated region and bare channel based on the data from Devi et al. [10] (see Table 2). Natural rice stems (*O. sativa*) were used to construct a patch with $b=50$ cm and $\varphi=0.01$. The vertical gray dashed line is the upstream edge of the natural rice patch

constant velocity inside the patch ($L > L_3$). In this case, $U_0=27$ cm/s and $\varphi=0.001$. The modeled velocities (lines in Fig. 9) effectively match the measured velocities (points in Fig. 9) inside the patch and bare channel, with an $RMSE=0.9$ cm/s.

Overall, in the vegetated region and bare channel, the modeled longitudinal profiles of the velocities agree well with measured velocities for model patches longer than (our study, White and Nepf [46], and Zong and Nepf [52]) or shorter than (Maji et al. [31] and Ben

Meftah and Mossa [33]) the interior adjustment distance, L_3 . The modeling result is more accurate than the results of a previous study (Fig. 6). Furthermore, this model can produce accurate longitudinal profiles of velocities in natural vegetation patches [10]. These findings indicate that the proposed model is capable of modeling longitudinal velocity profiles in vegetated regions and bare channels.

7 Discussion

7.1 Sensitivity analysis

Case A3 is taken as an example to examine the sensitivity of K_2 and K_3 in Eqs. (10) and (11), respectively. When K_2 or K_3 changes, all other parameters are fixed as specified in Table 1. First, we discuss the sensitivity of K_2 . In case A3, $K_2 = 1.5$, therefore, a wide range of K_2 ($= 0.1$ to 3) is considered. K_3 is fixed at 2 (Table 1). In the vegetated region, the modeling results are very sensitive to the K_2 value when K_2 is small (e.g., $K_3 = 0.1$, blue line in Fig. 10a), and a 16% overestimation is observed over the upstream and interior adjustment distances. Meanwhile, the velocity ($= 17.5$ cm/s) at the upstream edge of the patch ($x = 0$ cm) is overestimated relative to the measurement ($= 14.9$ cm/s). When $K_2 \geq 0.8$, the model becomes much less insensitive to K_2 and the modeling velocities are close to the

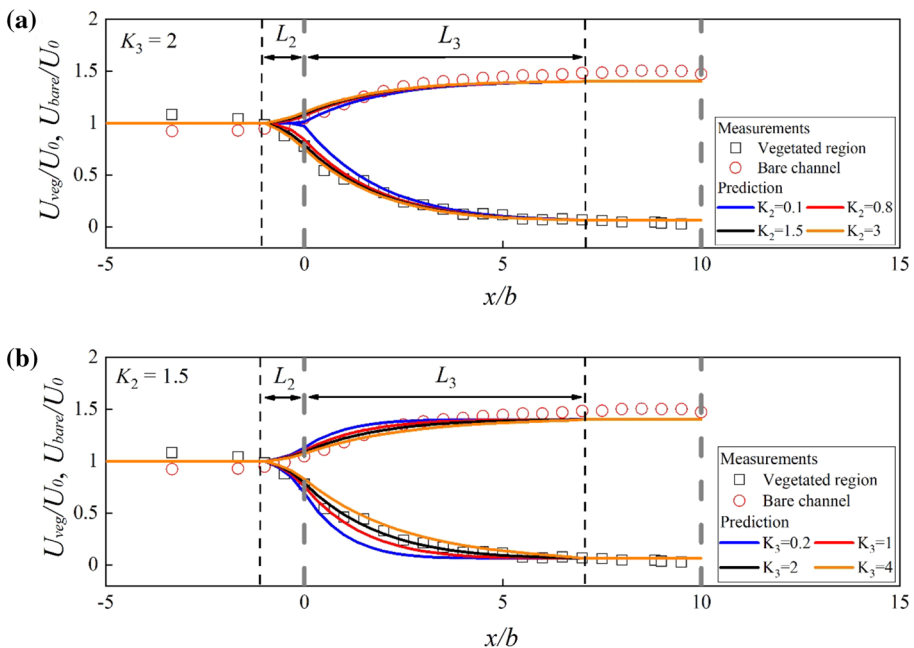


Fig. 10 Sensitivity analysis for two calibrated parameters, **a** K_2 and **b** K_3 , based on the data from case A1. When K_2 or K_3 changes, the other parameters are fixed, as specified in Table 1. The upstream and interior flow adjustment distances (L_2 and L_3) are given in the two subplots. The two vertical gray lines indicate the upstream and downstream edges of the model patch

measurements. Specifically, the difference between the predictions for $K_2=0.8$ and $K_2=3$ is less than 4%, and both lines (red and orange lines) match the measurements.

Next, the sensitivity of K_3 is discussed. In case A3, K_2 is fixed at 1.5 and K_3 is varied between 0.2 and 4 (Fig. 10b). In the vegetated region, the model is sensitive to K_3 over two flow adjustment regions (L_2 and L_3), particularly over L_3 , where a small K_3 (e.g., $K_3=0.2$, the blue line) leads to underestimated velocities. In contrast, a large K_3 (e.g., $K_3=4$, the orange line) corresponds to overestimated velocities. Therefore, good modeling can be obtained only if an appropriate K_3 value ($=2$, the black line) is chosen. Finally, compared to K_2 , the model is more sensitive to K_3 . Thus, we suggest choosing K_3 first and then determining K_2 .

In addition, the velocity trends in the vegetated region and bare channel are opposite. The modeled mean velocity in the bare channel is dependent on the patch and channel widths. In this study, the width of the bare channel ($B-b$) was wider than the half patch width (b); therefore, the modeled mean velocity in the bare channel is less sensitive than that in the vegetated region.

7.2 Model limitations

The proposed model has certain limitations. First, the current model has been verified over a wide range of parameters based on data from this study and published literature, i.e., the ratio of the patch to channel width, $b/B=27$ to 75%; the frontal area per patch volume, $a=0.012$ to 0.21 cm^{-1} ; the solid volume fraction, $\varphi=0.003$ to 0.1; the mean channel velocity, $U_0=5$ to 29 cm/s; the flow depth, $H=6.6$ to 18 cm. Beyond those ranges, further validation is needed. Second, our experiments and those in the published literature were performed in straight channels; thus, the current model cannot present a longitudinal profile of velocities in a different type of channel. For example, in a meandering channel with a patch of aquatic vegetation, secondary flows may change the flow adjustment inside and outside of the patch (e.g., [26, 27, 38, 39]).

Finally, this model is confirmed to be valid for a model patch (cylinder arrays or cylinder-like plant arrays) but cannot be directly applied for a patch of real plants. Specifically, most data for model validation were from cases with cylinder arrays (in our study; White and Nepf [46], Zong and Nepf [52], Maji et al. [31] and Ben Meftah and Mossa [33]). We only used one case (a natural rice, *O. sativa*) from Devi et al. [10] to verify the modeling result. Good modeling results were obtained because *O. sativa* has a similar configuration to that of a rigid cylinder, which did not exhibit significant deflection during the experiment. Note that for the patches with only one stream-parallel side, the flow development along the side edge may be altered due to stronger coherent structures (e.g., White and Nepf [46]). The enhanced vortices may have a negligible impact on the mean velocities of the vegetated region and bare channel because for one stream-parallel side patches (e.g., White and Nepf [46], Zong and Nepf [52]), the modeling velocities are consistent with the measurements (Fig. 7). In addition, a vegetation patch in a natural river or wetland area consists of real plants that may be more flexible and have more complex shapes such that the penetration distances of the KH vortices into the patch may be changed (e.g., plants with leaves, [4, 5, 9]). Inside the patch and in the adjacent bare channel, the vertical profiles of the streamwise velocities may deviate from the logarithmic profile, therefore, the mid-depth velocity may no longer be the same as the depth-averaged velocity. Accordingly, the proposed model should be verified using more data from cases with natural plants.

Therefore, we reiterate that the current model is valid for model patches of cylinders or cylinder-like plants.

8 Summary

In an open channel with a vegetation patch, a model was proposed for modeling the longitudinal profiles of velocities in both the vegetated region and bare channel. The current model includes two different dimensionless parameters in the flow adjustment regions upstream of and inside the patch. The longitudinal transect was divided into four regions, in which analytical solutions are proposed separately. The proposed model is verified to be capable of modeling the longitudinal profiles of velocities in the vegetated region and bare channel, regardless of whether fully developed flows were acquired or not inside the model patches. The model displayed a higher modeling accuracy than that in a previous study [29]. Finally, this model can provide accurate longitudinal profiles of velocities in channels with model patches of cylinders or cylinder-like plants.

Acknowledgments We would like to acknowledge financial support from the National Natural Science Foundation of China (Nos. 51879175 and 51709022), the Huo Hua Ku Program of Sichuan University (No. 2018SCUH0020).

References

1. Bouma TJ, Duren LAV, Temmerman S, Claverie T, Blanco-Garcia A, Ysebaert T, Herman PMJ (2007) Spatial flow and sedimentation patterns within patches of epibenthic structures: combining field, flume and modelling experiments. *Cont Shelf Res* 27(8):1020–1045. <https://doi.org/10.1016/j.csr.2005.12.019>
2. Biggs HJ, Nikora VI, Gibbins CN et al (2019) Flow interactions with an aquatic macrophyte: a field study using stereoscopic particle image velocimetry. *J Ecohydraul.* <https://doi.org/10.1080/24705357.2019.1606677>
3. Caroppi G, Gualtieri P, Fontana N, Giugni M (2020) Effects of vegetation density on shear layer in partly vegetated channels. *J Hydro-Environment Res.* <https://doi.org/10.1016/j.jher.2020.01.008>
4. Caroppi G, Västilä K, Järvelä J, Rowiński PM, Giugni M (2019) Turbulence at water-vegetation interface in open channel flow: experiments with natural-like plants. *Adv Water Resour* 127:180–191. <https://doi.org/10.1016/j.advwatres.2019.03.013>
5. Chembolu V, Kakati R, Dutta S (2019) A laboratory study of flow characteristics in natural heterogeneous vegetation patches under submerged conditions. *Adv Water Resour* 133:103418. <https://doi.org/10.1016/j.advwatres.2019.103418>
6. Cheng N, Hui C, Chen X (2019) Estimate of drag coefficient for a finite patch of rigid cylinders. *J Hydraul Eng* 145(2):060818019. [https://doi.org/10.1061/\(ASCE\)HY.1943-7900.0001561](https://doi.org/10.1061/(ASCE)HY.1943-7900.0001561)
7. Coon WF, Bernard JM, Seischab FK. (2000). Effects of a cattail wetland on water quality of irondequoit creek near rochester, New York (No. 2000–4032). US Geological Survey. <https://doi.org/10.3133/wri004032>
8. Cornacchia L, Van De Koppel J, Van Der Wal D, Wharton G, Puijalón S, Bouma TJ (2018) Landscapes of facilitation: how self-organized patchiness of aquatic macrophytes promotes diversity in streams. *Ecology* 99(4):832–847. <https://doi.org/10.1002/ecy.2177>
9. Da Silva Filho JA, Cantalice JRB, Guerrra SMS, dos Santos Nune EO et al (2019) Drag coefficient and hydraulic roughness generated by an aquatic vegetation patch in a semi-arid alluvial channel. *Ecol Eng* 141:105598. <https://doi.org/10.1016/j.ecoleng.2019.105598>
10. Devi TB, Sharma A, Kumar B (2018) Flow characteristics in a partly vegetated channel with emergent vegetation and seepage. *Ecohydrol Hydrobiol* 19:93–108. <https://doi.org/10.1016/j.ecohyd.2018.07.006>
11. Dieter CD (1990) The importance of emergent vegetation in reducing sediment resuspension in wetlands. *J Freshw Ecol* 5(4):467–473. <https://doi.org/10.1080/02705060.1990.9665263>

12. Grace JB, Harrison JS (1986) The biology of Canadian weeds. 73. *Typha latifolia* L., *Typha angustifolia* L. and *Typha xglauca* Godr. *Can J Plant Sci* 66:361–379. <https://doi.org/10.4141/cjps86-051>
13. Gu J, Shan Y, Liu C, Liu X (2019) Feedbacks of flow and bed morphology from a submerged dense vegetation patch without upstream sediment supply. *Environ Fluid Mech* 19(2):475–493. <https://doi.org/10.1007/s10652-018-9633-5>
14. Hu Z, Lei J, Liu C, Nepf H (2018) Wake structure and sediment deposition behind models of submerged vegetation with and without flexible leaves. *Adv Water Resour* 118:28–38. <https://doi.org/10.1016/j.advwatres.2018.06.001>
15. Huai W, Xu Z, Yang Z, Zeng Y (2008) Two dimensional analytical solution for a partially vegetated compound channel flow. *Appl Math Mech* 29(8):1077–1084. <https://doi.org/10.1007/s10483-008-0811-y>
16. Huai W, Xue W, Qian Z (2015) Large-eddy simulation of turbulent rectangular open-channel flow with an emergent rigid vegetation patch. *Adv Water Resour* 80:30–42. <https://doi.org/10.1016/j.advwatres.2015.03.006>
17. Huai W, Song S, Han J, Zeng Y (2016) Prediction of velocity distribution in straight open-channel flow with partial vegetation by singular perturbation method. *Appl Math Mech* 37(10):1315–1324. <https://doi.org/10.1007/s10483-016-2135-9>
18. Kim HS, Kimura I, Park M (2018) Numerical simulation of flow and suspended sediment deposition within and around a circular patch of vegetation on a rigid bed. *Water Resour Res*. <https://doi.org/10.1029/2017wr021087>
19. Kim HS, Kimura I, Shimizu Y (2015) Bed morphological changes around a finite patch of vegetation. *Earth Surf Proc Land* 40(3):375–388. <https://doi.org/10.1002/esp.3639>
20. Knight DW, Omran M, Tang X (2007) Modeling depth-averaged velocity and boundary shear in trapezoidal channels with secondary flows. *J Hydraul Eng* 133(1):39–47. [https://doi.org/10.1016/\(asce\)0733-9429\(2017\)133:1\(39\)](https://doi.org/10.1016/(asce)0733-9429(2017)133:1(39))
21. Leonard LA, Luther ME (1995) Flow hydrodynamics in tidal marsh canopies. *Limnol Oceanogr* 40(8):1474–1484. <https://doi.org/10.4319/lo.1995.40.8.1474>
22. Licci S, Nepf H, Delolme C et al (2019) The role of patch size in ecosystem engineering capacity: a case study of aquatic vegetation. *Aquatic Sci*. <https://doi.org/10.1007/s00027-019-0635-2>
23. Lightbody AF, Nepf H (2006) Prediction of velocity profiles and longitudinal dispersion in salt marsh vegetation. *Limnol Oceanogr* 51(1):218–228. <https://doi.org/10.4319/lo.2006.51.1.0218>
24. Liu C, Luo X, Liu X, Yang K (2013) Modeling depth-averaged velocity and bed shear stress in compound channels with emergent and submerged vegetation. *Adv Water Resour* 60:148–159. <https://doi.org/10.1016/j.advwatres.2013.08.002>
25. Liu C, Nepf H (2016) Sediment deposition within and around a finite patch of model vegetation over a range of channel velocity. *Water Resour Res* 52(1):600–612. <https://doi.org/10.1002/2015WR018249>
26. Liu C, Shan Y, Liu X, Yang K, Liao H (2016) The effect of floodplain grass on the flow characteristics of meandering compound channels. *J Hydrol* 542:1–17. <https://doi.org/10.1016/j.jhydrol.2016.07.037>
27. Liu C, Hu Z, Lei J, Nepf H (2018) Vortex structure and sediment deposition in the wake behind a finite patch of model submerged vegetation. *J Hydraul Eng* 144(2):04017065. [https://doi.org/10.1061/\(ASCE\)HY.1943-7900.0001408](https://doi.org/10.1061/(ASCE)HY.1943-7900.0001408)
28. Liu X, Zhou Q, Huang S, Guo Y, Liu C (2018) Estimation of flow direction in meandering compound channel. *J Hydrol* 556:143–153. <https://doi.org/10.1016/j.jhydrol.2017.10.071>
29. Liu C, Shan Y (2019) Analytical model for predicting the longitudinal profiles of velocities in a channel with a model vegetation patch. *J Hydrol* 576:561–574. <https://doi.org/10.1016/j.jhydrol.2019.06.076>
30. Liu C, Shan Y, Sun W, Yan C, Yang K (2020) An open channel with an emergent vegetation patch: predicting the longitudinal profiles of velocities based on exponential decay. *J Hydrol* 582:124429. <https://doi.org/10.1016/j.jhydrol.2019.124429>
31. Maji S, Debasish P, Prashanth RH, Umesh PG (2016) Hydrodynamics and turbulence in emergent and sparsely vegetated open channel flow. *Environ Fluid Mech* 17(4):853–877. <https://doi.org/10.1007/s10652-017-9531-2>
32. Malmon DV, Dunne T, Reneau SL (2002) Predicting the fate of sediment and pollutants in river floodplains. *Environ Sci Technol* 36(9):2026–2032. <https://doi.org/10.1021/es010509>
33. Meftah MB, Mossa M (2016) A modified log-law of flow velocity distribution in partly obstructed open channels. *Environ Fluid Mech* 16(2):453–479. <https://doi.org/10.1007/s10652-015-9439-7>
34. Nicollea E (2011) Numerical study of flow through and around a circular array of cylinders. *J Fluid Mech* 679:1–31. <https://doi.org/10.1017/jfm.2011.77>
35. Ren B, Wang D, Li W, Yang K (2019) The velocity patterns in rigid and mobile channels with vegetation patches. *J Hydrodyn*. <https://doi.org/10.1007/s42241-019-0067-4>

36. Rominger JT, Nepf H (2011) Flow adjustment and interior flow associated with a rectangular porous obstruction. *J Fluid Mech* 680:636–659. <https://doi.org/10.1017/jfm.2011.199>
37. Sand-Jensen K, Pedersen ML (2008) Streamlining of plant patches in streams. *Freshwater Biol* 53(4):714–726. <https://doi.org/10.1111/j.1365-2427.2007.01928.x>
38. Shan Y, Liu X, Yang K, Liu C (2017) Analytical model for stage-discharge estimation in meandering compound channels with submerged flexible vegetation. *Adv Water Resour* 108:170–183. <https://doi.org/10.1016/j.advwatres.2017.07.021>
39. Shan Y, Huang S, Liu C, Guo Y, Yang K (2018) Prediction of the depth-averaged two-dimensional flow direction along a meander in compound channels. *J Hydrol* 565:318–330. <https://doi.org/10.1016/j.jhydrol.2018.08.004>
40. Shan Y, Chao L, Nepf H (2019) Comparison of drag and velocity in model mangrove forests with random and in-line tree distributions. *J Hydrol* 568:735–746. <https://doi.org/10.1016/j.jhydrol.2018.10.077>
41. Shan Y, Zhao T, Liu C, Nepf H (2020) Turbulence and bed-load transport in channels with randomly distributed emergent patches of model vegetation. *Geophys Res Lett*. <https://doi.org/10.1029/2020GL087055>
42. Schoelynck J et al (2012) Self-organised patchiness and scale-dependent bio-geo- morphic feedbacks in aquatic river vegetation. *Ecography* 35(8):760–768. <https://doi.org/10.1111/j.1600-0587.2011.07177.x>
43. Temmerman S, Bouma TJ, Govers G et al (2005) Impact of vegetation on flow routing and sedimentation patterns: Three-dimensional modeling for a tidal marsh. *J Geophys Res Earth Surface* 110:F04019. <https://doi.org/10.1029/2005jf000301>
44. Vandenbruwaene W, Temmerman S, Bouma TJ, Klaassen PC, De Vries MB, Callaghan DP, Meire P (2011) Flow interaction with dynamic vegetation patches: Implications for biogeomorphic evolution of a tidal landscape. *J Geophys Res Earth Surface* 116(F1):155–170. <https://doi.org/10.1029/2010jf001788>
45. Wang W, Huai W, Li S, Wang P, Wang Y, Zhang J (2019) Analytical solutions of velocity profile in flow through submerged vegetation with variable frontal width. *J Hydrol* 578:124088. <https://doi.org/10.1016/j.jhydrol.2019.124088>
46. White BL, Nepf H (2008) A vortex-based model of velocity and shear stress in a partially vegetated shallow channel. *Water Resour Res*. <https://doi.org/10.1029/2006WR005651>
47. Widdows J, Pope ND, Brinsley MD (2008) Effect of *Spartina anglica* stems on near-bed hydrodynamics, sediment erodability and morphological changes on an intertidal mudflat. *Mar Ecol Prog Ser* 362:45–57. <https://doi.org/10.3354/meps07448>
48. Wu C (2016) *Hydraulics*. Higher Education Press, Beijing
49. Yang K, Cao S, Knight DW (2007) Flow patterns in compound channels with vegetated floodplains. *J Hydraul Eng* 133(2):148–159. [https://doi.org/10.1061/\(ASCE\)0733-9429\(2007\)133:2\(148\)](https://doi.org/10.1061/(ASCE)0733-9429(2007)133:2(148))
50. Yamasaki TN, de Lima PHS, Nepf H et al (2019) From patch to channel scale: the evolution of emergent vegetation in a channel. *Adv Water Resour* 129:131–145. <https://doi.org/10.1016/j.advwatres.2019.05.009>
51. Zhang J, Zhong Y, Huai W (2018) Transverse distribution of streamwise velocity in open-channel flow with artificial emergent vegetation. *Ecol Eng* 110:78–86. <https://doi.org/10.1016/j.ecoleng.2017.10.010>
52. Zong L, Nepf H (2011) Spatial distribution of deposition within a patch of vegetation. *Water Resour Res* 47:W03516. <https://doi.org/10.1029/2010WR009516>

Publisher's Note Springer Nature remains neutral with regard to jurisdictional claims in published maps and institutional affiliations.